Supporting Information
for

Surface Modified Copper Foam with Cobalt Phthalocyanine Carbon Nanotube Hybrids for Tuning CO_2 Reduction Reaction Products

Javier O. Rivera-Reyes[a,b], Keith J. Billings[c], Carmen L. Metzler[a,b], Richard M. Lagle[d], Mebougna Drabo[d], Ratnakar Palai[e], John-Paul Jones[c], Dalice M. Piñero Cruz[a,b]

[a]Chemistry Department, College of Natural Sciences, Rio Piedras Campus, University of Puerto Rico, San Juan, PR 00931-3346, USA
[b]Molecular Science Research Center, University of Puerto Rico, 1390 Ponce de León, San Juan, PR 00926, USA
[c]Jet Propulsion Laboratory, California Institute of Technology, Pasadena, CA 91109, USA
[d]Department of Mechanical Engineering, Alabama A&M University, Huntsville, Alabama 35762, USA
[e]Department of Physics, College of Natural Sciences, Rio Piedras Campus, University of Puerto Rico, San Juan, PR 00936, USA

1. Materials and Methods

1.1 General

All materials were purchased from Sigma Aldrich, Fisher Scientific, and Dioxide Materials. The used copper foam was acquired from American Elements. All materials were used as purchased unless otherwise stated. Thermogravimetric analysis (TGA) was collected with a TA instrument TGA 5500 using a 20 ^{o}C/min ramp under inert atmosphere (N_2). Powder X-ray diffraction (PXRD) was used to evaluate the structural properties on a PANalytical Aeris instrument. Raman spectra were collected on a Thermo Scientific DXR Raman Imaging Microscope. The morphological characterization of the reported materials was done by scanning electron microscopy (SEM) on a JEOL JSM-6480LV at operating conditions of 20 kV. X-ray photoelectron spectroscopy (XPS) surface analysis was measured using a Thermo Fisher manufacture instrument with an Al K-Alpha monochromatic source (1486.68 eV). The Co concentration of the CoPc hybrid was determined using an ICP – OES Optima 8000 Perkin Elmer equipment, with standard plasma parameters. The samples were prepared by dissolving ~5 mg in HNO_3 (BAKER INSTRA-ANALYZED Reagent,70% for trace metal analysis) and lightly heated. The obtained solution was allowed to cool down before diluting with 2% HNO_3 and followed by ICP-OES analysis.

1.2 Hybrid material preparation

The multi-walled carbon nanotubes (MWCNTs) were functionalized with COOH groups by heating them to 70 ^{o}C in a (3:1) HNO_3:H_2SO_4 solution for 2 hours. The functionalized MWCNTs were centrifuged and washed thoroughly with DI water to remove all acid residue. Then the black solid was dried under vaccum overnight to yield the f-MWCNT. To prepare the hybrid materials equal amounts of f-MWCNTs and CoPc were weighted in separate vials. The f-MWCNTs were dispersed in DMF solution, and it was sonicated for 15 minutes, and CoPc was dissolved in DMF/acetone assisted by sonication. Afterwards the CoPc solution was added dropwise to the f-MWCNTs dispersion, and this resulting solution was sonicated for 15 minutes and vigorously stirred overnight. The hybrid solution was centrifuge at 5000 rpm washed with acetone and water several times and dried under vacuum at 100 °C overnight.

1.3 Electrode preparation:

The cathode was prepared by dispersing 5 mg of the prepared hybrid material in 4 mL of (2:1:1) MeOH:H_2O:i-PrOH by sonication of 30 minutes. 10% of Nafion was added as a binder and the resulting solution was sonicated an additional 10 minutes. The prepared ink was spray coated on a rolled down Cu foam to 7 mm a cut (2.25 x 2.25 cm) to obtain a 1 mg/cm^2 mass loading. The anode was prepared by dispersing iridium oxide in a (1:1) H_2O:i-PrOH solution with 10% Nafion binder. The resulting anode ink was spray coated onto a Pt/Ti fiber felt (2.5 x 2.5 cm) to obtain a 1 mg/cm^2 mass loading anode electrode.

1.4 Cell design, electrolysis studies, CO_2RR product characterization

The electrolyzer cell consists of an anode and cathode plates made of stainless steel and titanium, gasket materials, and a membrane electrode assembly. The electrode plates have dimensions of 7.62 x 7.62 x 1 cm and a 5 cm^2 slot for the placement of the electrodes. The active area slot contains a serpentine path for the delivery of the gas and liquid feed to the back of the electrodes. In between the electrodes an anion exchange membrane (Sustainion^{TM} 37-50 RT) is placed to separate both electrodes and allow the permeation of negative charge ions. The gasket materials were all cut to similar thickness of the electrode materials and the eight bolts of the cell were initially tightened in a cross manner to 15 lb/in and further tightened to 25 lb/in. The CO_2 is delivered to the cathode at a flow rate of 100 standard cubic centimeter per minute (sccm) before reaching the cathode the CO_2 is

passed through a water to humified it. In the case of the anode the 100 mM $KHCO_3$ is cycled using a peristaltic pump. Chronoamperometry experiments were performed using a Gamry Interface 5000E potentiostat. The gas chromatography (GC) experiments were performed using an SRI Model 8610C instrument previously calibrated using a calibration gas from Airgas and measurements were taken periodically. The GC has a flame ionization detector (FID) equipped with a methanizer allowing for the detection and quantification CO, CH_4, and C_2H_4. The thermal conductivity detector (TCD) equipped to the GC is used for the quantification of H_2. The GC is equipped with a 0.5-meter Haysep-D precolumn, 2-meter MoleSieve 5A column, and a 2-meter Haysep D column.

The Faradaic efficiency of the formed products (FE_{prod}) was determined by using the following equation:

$$FE_{prod} = \frac{n \times F \times X_{prod} \times \nabla}{I} \times 100$$

where n is the number of electrons transferred, F is Faraday's constant 96485 C/mol, X_{prod} is the molar fraction of the product, ∇ is the molar flow rate of the products (mol/s), and I is the current measured in amperes.

The $EE_{full\ cell}$ was measured using the following equation[1]:

$$EE_{full\ cell} = \frac{E^{\circ}_{ox} - E^{\circ}_{red}}{E_{full\ cell}} xFE$$

where E°_{ox} and E°_{red} are the water oxidation and CO_2RR thermodynamic potential, and $E_{full\ cell}$ is the applied full cell voltage.

CO = -0.10 V SHE

CH_4 = -0.24 V SHE

C_2H_4 = -0.28 V vs SHE

2. Characterization

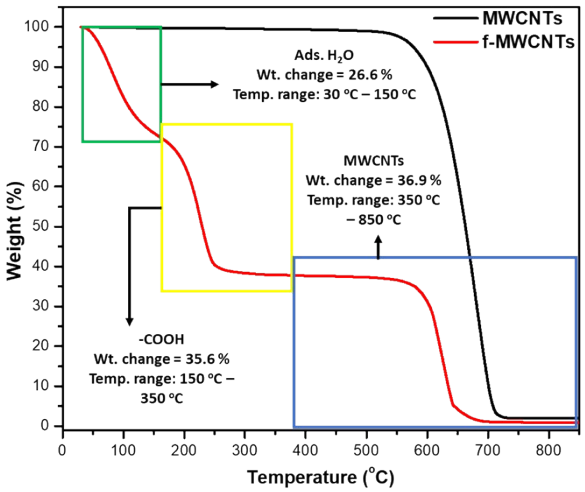

Figure S1. TGA weight percent loss of pre-acid and post-acid treatment of MWCNTs.

The f-MWCNTs presented three thermal decomposition zones confirming the successful addition of the -COOH groups to the MWCNTs surface (fig. S1). The first zone observed has a 26.6 % weight change ranging from 30 °C to 150 °C and it is ascribed to adsorbed water to the f-MWCNTs.[2] The second zone is attributed to decarboxylation of the COOH moieties on the MWCNTs surface the total weight loss in this stage was of 35.4 % and it started around 200 °C.[2–4] The third and final thermal degradation zone is assigned to carbon nanotubes and the weight loss becomes apparent after reaching temperatures slightly above 600 °C. In addition, TGA was also used to confirm the incorporation of the metal phthalocyanines to the f-MWCNTs.

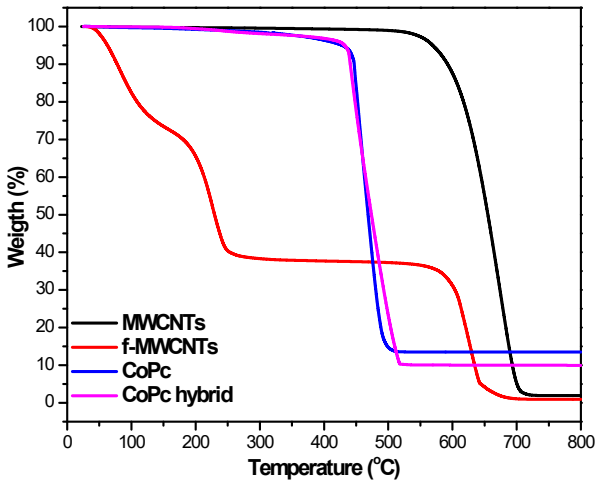

Figure S2. TGA weight percent loss of MWCNTs, f-MWCNTs, CoPc, and CoPc hybrids.

Table S1. CoPc content in the hybrid material determined by ICP-OES.

Sample	CoPc/f-MWCNTs weight ratio before mixing	Metal	CoPc content (% wt)
CoPc hybrid	1:1	Co	60.1

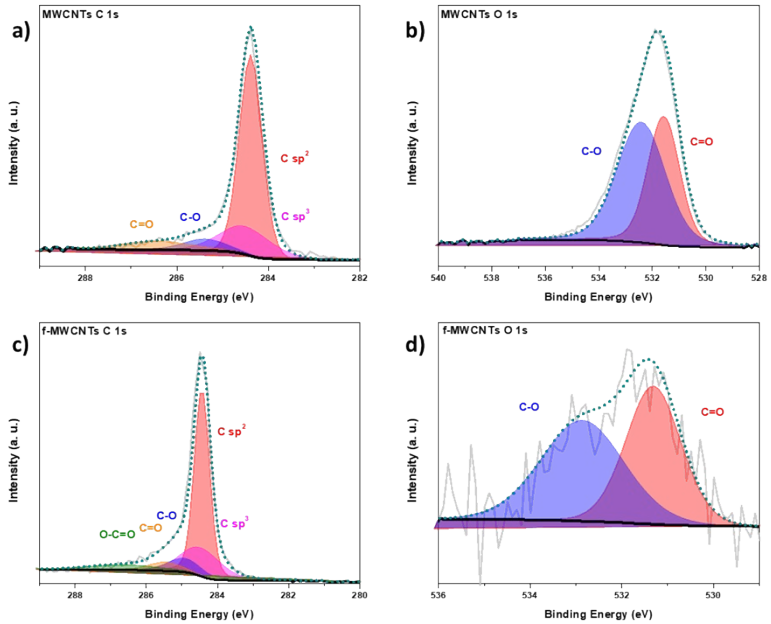

Figure S3. a) – b) XPS spectra of MWCNTs; a) C 1s and O 1s. c) – d) XPS spectra of f-MWCNTs; a) C 1s and O 1s.

XPS surface analysis of the MWCNTs before and after acid functionalization is shown in fig. S3. As expected, the chemical composition of the MWCNTs is mainly carbon. The C 1s peak in the MWCNTs can be deconvoluted into 4 distinct signals representing C sp^2 (284.4 eV), C sp^3 (284.6 eV), C-O (285.4 eV), and C=O (286.4 eV) (fig. S3 a)). In fig. S4 b), the O 1s scan confirms the presence of C-O and C=O at 532.4 eV and 531.6 eV, respectively. However, after acidification, a new band appears in the C 1s spectra corresponding to O-C=O (fig. S3 c)). Furthermore, the C=O band increases after acidification, compared to the as-received MWCNTs. Similarly, the O 1s scan of the f-MWCNTs in fig S3 d) shows an increased C=O band, confirming the surface functionalization of the MWCNTs.[5,6]

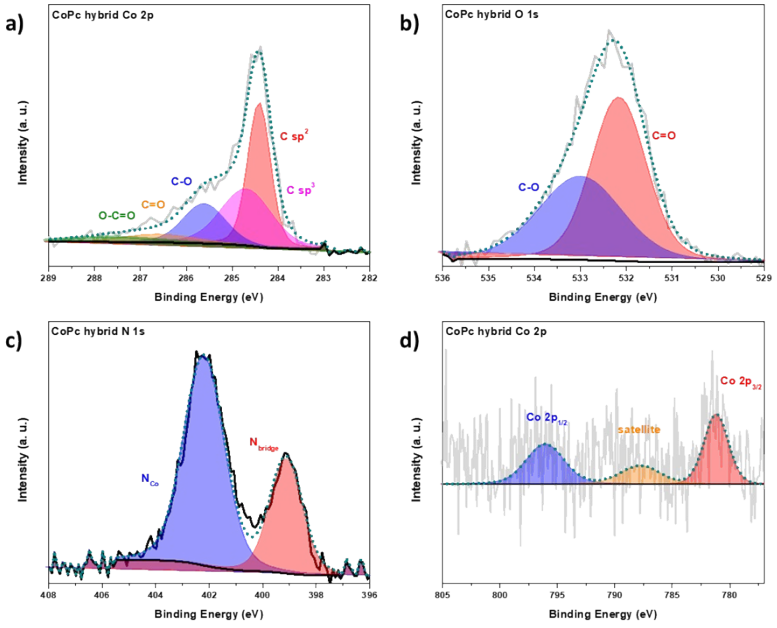

Figure S4. XPS of CoPc hybrid a) C1 s spectra, b) O 1s spectra, c) N 1s spectra, and d) Co 2p spectra.

The CoPc hybrid C 1s XPS spectrum in fig. S4 a), showed similar peaks to one observed previously. In the O 1s spectrum (fig. S4 b)) the C-O and C=O peaks shifted to higher binding energy suggesting

successful loading of the CoPc and of the f-MWCNTs.[7] Additionally, the N 1s spectrum of the CoPc hybrid exhibits the characteristic N peaks of the CoPc attributed to the bridging N and coordinated N (fig. S4 c)).[7] The Co 2p spectra in fig. S4 d), shows the Co $2p_{3/2}$ and $2p_{1/2}$ peaks associated to the CoPc at 781.2 eV and 796.1 eV, respectively.

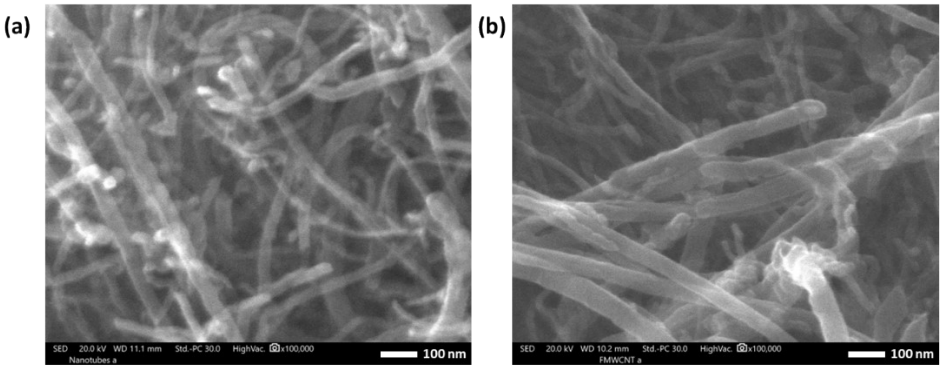

Figure S5. SEM images of a) MWCNTs, and b) f-MWCNTs.

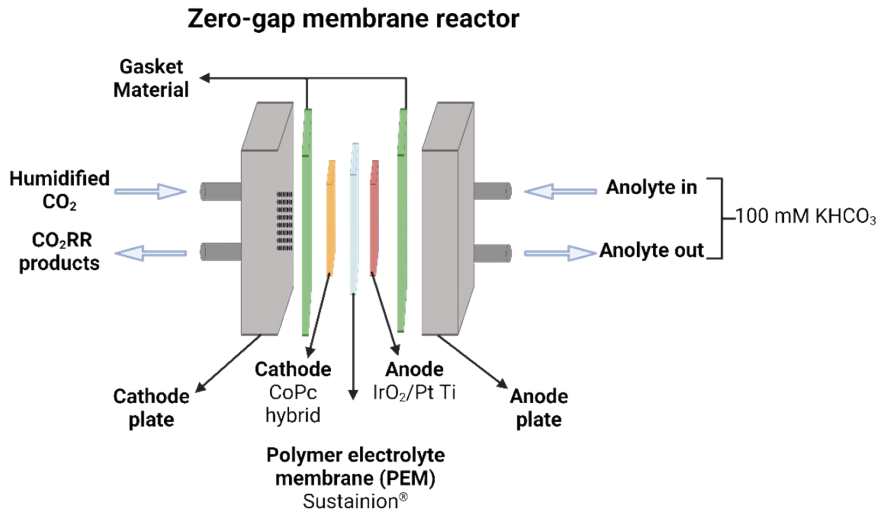

Figure S6. Schematic diagram of the zero-gap membrane reactor. Created with Biorender.com

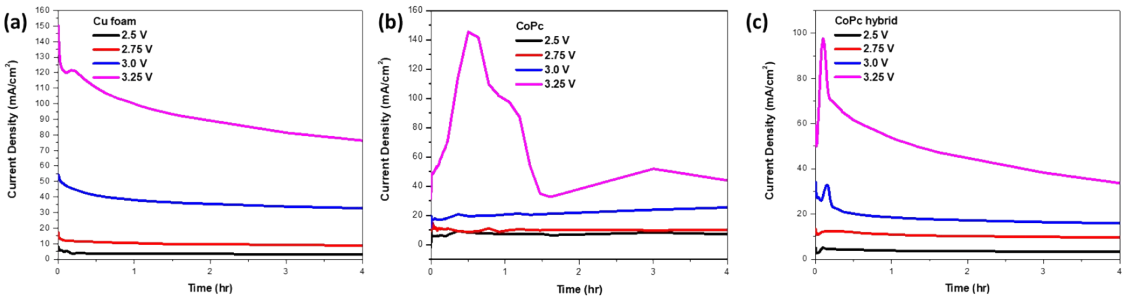

Figure S7. Chronoamperograms curves of a) Cu foam, b) bare CoPc modified Cu foam, and c) CoPc hybrid modified Cu foam.

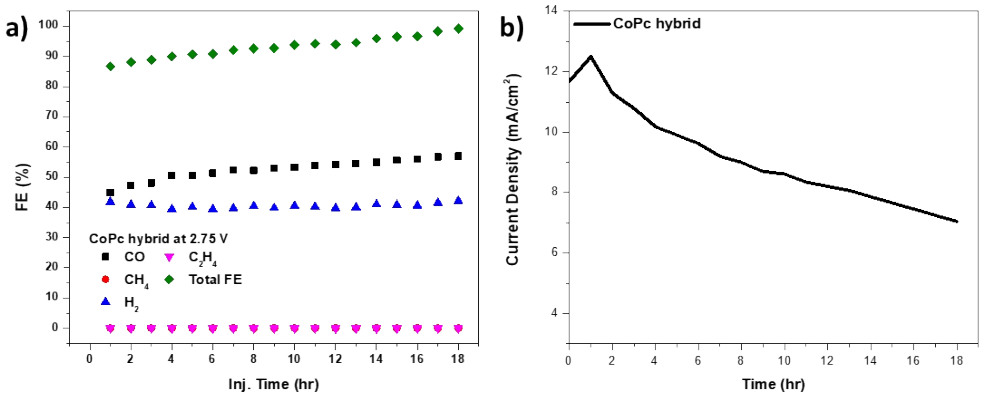

Figure S8. CoPc hybrid modified Cu foam a) faradaic efficiency and b) chronoamperogram at 2.75 V throughout the 18-hour stability study.

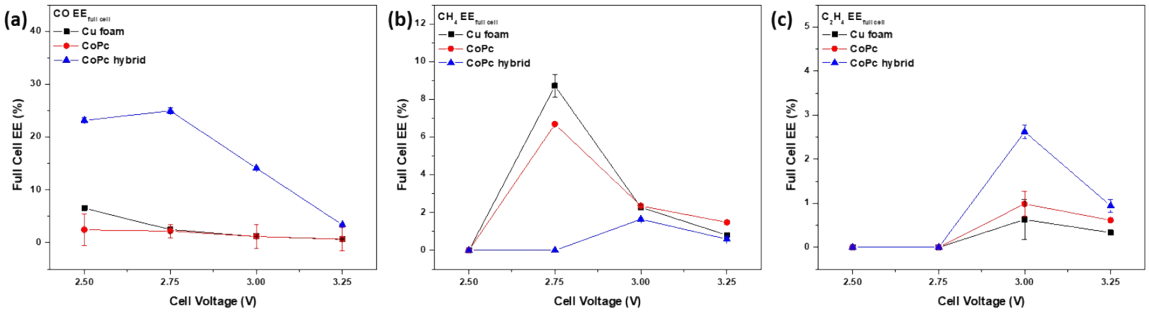

Figure S9. $EE_{full\ cell}$ for a) CO, b) CH_4, and C_2H_4.

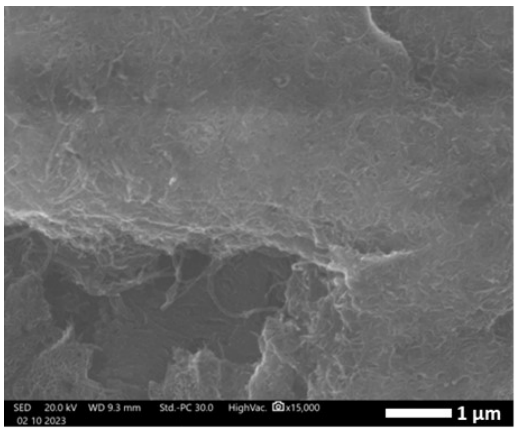

Figure S10. SEM image after electrolysis of CoPc hybrid.

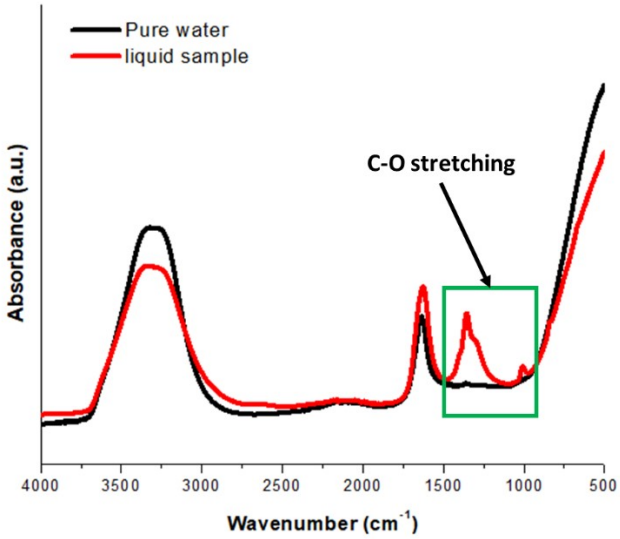

Figure S11. FTIR of collected liquid products.

Table S2. Comparison of CO_2RR performance against similar published work.

Material	Substrate	Potential (V)	FE_{H2} (%)	Major CO_2RR product (FE%)	Reference
Bare Cu foam	Cu foam	2.75 V	58	CH_4 (14%)	This work
CoPc	Cu foam	2.75 V	30	CH_4 (13%)	
CoPc hybrid (COOH-MWCNTs)	Cu foam	2.75 V	28	CO (51%)	
FeTPP[Cl]	PTFE/Cu sputtering	3 V – 3.7 V	~5	EtOH (~41%) and C_2H_4 (~40%)	[1]
CoPc/COOH MWCNTs	Carbon paper	-0.6 V vs RHE	5 to 25 (after 10 hours)	CO (90% to 75%)	[7]
Cu flow through GDE (FTGDE)	Cu FTGDE	-0.7 to -1.1 V vs RHE	~15	Formate (76%)	[8]

3. References

1 F. Li, Y. C. Li, Z. Wang, J. Li, D.-H. Nam, Y. Lum, M. Luo, X. Wang, A. Ozden, S.-F. Hung, B. Chen, Y. Wang, J. Wicks, Y. Xu, Y. Li, C. M. Gabardo, C.-T. Dinh, Y. Wang, T.-T. Zhuang, D. Sinton and E. H. Sargent. *Nat. Catal.*, 2019, **3**, 75–82.

2 V. Datsyuk, M. Kalyva, K. Papagelis, J. Parthenios, D. Tasis, A. Siokou, I. Kallitsis and C. Galiotis. *Carbon*, 2008, **46**, 833–840.

3 L. Thi Mai Hoa. *Diam. Relat. Mater.*, 2018, **89**, 43–51.

4 G. Vuković, A. Marinković, M. Obradović, V. Radmilović, M. Čolić, R. Aleksić and P. S. Uskoković. *Appl Surf Sci*, 2009, **255**, 8067–8075.

5 S. Kundu, Y. Wang, W. Xia and M. Muhler, *J. Phys. Chem. C*, 2008, **112**, 16869–16878.

6 D. V. Sivkov, O. V. Petrova, S. V. Nekipelov, A. S. Vinogradov, R. N. Skandakov. K. A. Bakina. S. I. Isaenko, A. M. Ob'edkov, B. S. Kaverin, I. V. Vilkov and V. N. Sivkov. *Applied Appl. Sci.* 2022, **12**, 7744.

7 H. Li, Y. Pan, Z. Wang, Y. Yu, J. Xiong, H. Du, J. Lai, L. Wang and S. Feng. *Nano. Res.*, 2022, **15**, 3056–3064.

8 A. Mustafa, B. G. Lougou, Y. Shuai, Z. Wang, Haseeb-ur-Rehman, S. Razzaq, W. Wang, R. Pan and J. Zhao. *Front. Chem. Sci. Eng.*, 2024, **18**, 29.